The Large Adaptive Reflector: A Giant Radio Telescope with an Aero Twist

Peter Dewdney * Meyer Nahon ** Bruce Veidt *

ABSTRACT

A multi-national grouping of radio astronomers has identified the need for a major new instrument, called the Square Kilometer Array (SKA), to be constructed in the coming decade. This giant radio telescope will be 100 times more powerful than any in existence today. The innovative Canadian concept for the underlying design of the telescope, the Large Adaptive Reflector (LAR), is among the best candidates and is well positioned to be adopted by the international community. The LAR is a concept for a low-cost, large-aperture, wideband, radio telescope, designed to operate over the wavelength range from 2 m to 1.4 cm. The proposed design for the LAR includes two central components. The first is a long focal length, large-diameter parabolic reflector, composed of actuated hexagonal panels, mounted on the ground. The second component is a focal package supported at a height of 500 m by a large helium balloon (aerostat) and a system of three or more taut tethers. The telescope is steered by simultaneously changing the lengths of the tethers with winches (thus changing the position of the feed) and by modifying the shape of the reflector. Simulations have shown that in operating wind conditions, the position of the feed platform can be stabilized to within a few centimetres. This paper gives an overview of the present state of the LAR design, with an emphasis on the airborne subsystem. Construction of a 1/3-scale model of the tethered aerostat subsystem, with a footprint of "only" 0.5 km^2, is presently underway in Penticton, B.C. It will allow a validation of the underlying design and the study of some fascinating issues in the design and control of this system.

Continued on page 240

* Herzberg Institute of Astrophysics
National Research Council Canada
P.O. Box 248
Penticton, BC V2A 6K3, Canada.

** Department of Mechanical Engineering
McGill University
817 Sherbrooke St. W.
Montreal, QC H3A 2K6, Canada.
(e-mail: meyer.nahon@mcgill.ca).
Received 12 June 2002.

1. INTRODUCTION

New developments in all fields of astronomy have brought the current generation of astronomers to the brink of understanding the origin and evolution of the Universe. The next major step – to explore the earliest epochs of the evolution of the Universe, before the dawn of first light and the creation of stars and galaxies – will require a giant telescope operating at radio wavelengths.

An international consortium of radio astronomers and engineers has agreed to investigate technologies to build the Square Kilometer Array (SKA), a cm-to-m-wave radio telescope for the next generation of investigation into cosmic phenomena. A looming "sensitivity barrier" will prevent current telescopes from making much deeper inroads at these wavelengths, particularly in studies of the early Universe. The aim of the SKA project is to increase the collecting area, the fundamental factor governing sensitivity, over existing telescopes by two orders of magnitude. As is the case with some other radio telescopes, the Canadian proposal for the SKA design consists of an array of 30–50 individual antennas whose signals are combined to yield the resolution of a much larger antenna. Each of these antennas would use the Large Adaptive Reflector (LAR) concept put forward by a group led by the National Research Council of Canada and supported by university and industry collaborators (Legg, 1998).

The LAR design is applicable to telescopes up to several hundred metres in diameter. However, for the purposes of illustration, this paper focuses on a specific 200-m implementation of the LAR design. **Figure 1** is an artist's concept of an LAR installation with details showing a main reflector section and a phased-array feed concept. Before the SKA is constructed, a single 200-m LAR prototype will be a powerful radio telescope in its own right with sensitivity and active collecting area on par with Arecibo (Gordon and Lalonde, 1961) but with a wider frequency range, essentially all-sky coverage, and wide field-of-view. Research on the LAR in Canada started with a preliminary study (Carlson et al., 2000) to find reasonable design solutions that would meet all of the requirements. Emphasis has now shifted to construction and testing of critical (perhaps scaled) elements of the LAR to determine if they will meet the design requirements.

suite de la page 239

RÉSUMÉ

Un groupe multinational de radioastronomes a besoin d'un nouvel instrument majeur appelé réseau de radiotélescopes SKA dont la construction sera réalisée au cours de la prochaine décennie. Ce radiotélescope géant sera 100 fois plus puissant que tout autre instrument utilisé dans le monde aujourd'hui. Le concept novateur canadien qui sous tend la conception du télescope, le grand réflecteur adaptatif (LAR pour Large Adaptive Reflector), figure parmi les meilleures propositions et a toutes les chances d'être adopté par la communauté internationale. Le LAR repose sur un concept de radiotélescope à large bande, à grande ouverture et peu coûteux conçu pour fonctionner dans la plage des longueurs d'onde de 2 m à 4 m. La conception proposée pour le grand réflecteur adaptatif repose sur deux composantes principales. La première est un réflecteur parabolique de grand diamètre et à longue distance focale constitué de panneaux hexagonaux commandés et montés au sol. La deuxième composante est un récepteur maintenu à une hauteur de 500 m par un gros ballon gonflé à l'hélium (aérostat) et un système d'au moins trois laisses tendues. Le télescope est manœuvré en modifiant simultanément la longueur des laisses à l'aide de treuils (modifiant ainsi l'alimentation) et en changeant la forme du réflecteur. Les simulations montrent que dans les conditions d'exploitation, la position de la plate-forme d'alimentation peut être stabilisée à quelques centimètres près. Le présent document donne un aperçu de l'état actuel de la conception du LAR, en mettant l'accent sur le sous-système aéroporté. La construction d'un modèle à l'échelle 1/3 du sous-système de l'aérostat en laisse, avec une empreinte de « seulement » 0.5 km^2, est présentement en cours à Penticton, C.-B. Ce modèle permettra de valider la conception fondamentale du réseau et l'étude de certains aspects fascinants touchant la conception et la commande de ce système.

2. The Main Reflector

The main reflector is a 200-m diameter actuated parabolic section. Its surface is actuated to maintain a shape equivalent to a standard offset parabolic antenna. As illustrated in **Figure 2**, it is essentially part of a much larger "virtual" parabola, which changes shape as the telescope is pointed in different directions. The pointing direction is defined by a Zenith Angle, θ_{za}, and an Azimuth Angle, θ_{az}. The distance from the centre of the reflector to the feed is denoted by R. At $\theta_{za} = 0$, we have $R = f$, where f is the focal length of the paraboloid. This geometry provides an unblocked aperture, except near $\theta_{za} = 0$. There are no scattering objects in the ray path from the sky to the focus, except occasionally one of the tethers, which is not expected to have measurable scattering. The "clean optics" presented by this design will be helpful for making precise measurements and for rejecting sky-borne interference.

The preliminary study concluded that the optimum focal ratio at $\theta_{za} = 0$ is about 2.5 (R = 500 m for a 200-m reflector diameter). This conclusion is based on a trade-off in an evaluation of many parameters, including feed stability, actuator throw, main-reflector panel size, feed size, and footprint of the telescope installation. Of particular interest is the maximum actuator stroke, which occurs along the y-axis (out of the page in **Figure 2**). The required stroke for these parameters is about 7 m.

Cost is a major issue in designing the main reflector. It is estimated that the cost per m^2 of surface will be much lower than for an equivalent-standard parabolic reflector, where the entire reflector must be tilted to large angles. Here the cost per unit area does not increase quickly with diameter. In the present design, large primary actuators support triangular space frames that form the main structure of the surface. These actuators are shared by neighbouring space frames. Reflector panels, proposed to be constructed of a low-density concrete composite, are supported by short stroke (10–15 cm) secondary actuators that provide final surface adjustment. The details are described in the following sections. Since the design of the reflector panels strongly influences the design of the support structure, they are described first.

2.1. Reflector Panels

The complete main reflector will contain about 150 triangular reflector sections, such as the one shown in the lower part of **Figure 1**. Each triangular section is 20 m on a side and consists of 10 hexagonal panels, each approximately 5 m in diameter, supported by a space frame. Thus, there will be about 1500 panels in a 200 m diameter main reflector. The requirements for the hexagonal reflector panels are that they be inexpensive, easy to construct, and stiff enough to meet the surface accuracy requirements for operation at a wavelength of 1.4 cm (rms surface accuracy of about 0.7 mm). Because of the long focal length, the panels can be fixed shape (nearly flat) and need not be particularly light, since they are supported directly by the ground. A concrete-and-steel construction ensures that wind-induced deflections will be negligible. A possible construction technique is to construct the panels of steel-fiber-reinforced concrete (SFRC) with an embedded steel frame. Once the panel has cured, the radio-reflecting surface, such as a spray-on, "self-healing" zinc coating, is applied. This design comes close to meeting the accuracy specifications, including thermal deformations. Alternative designs and cost-effective materials for the panels are also being considered with the goal of further reducing the cost of the main reflector structure.

2.2. Secondary (Short-Stroke) Actuator

The reflector panels are supported by short-stroke secondary actuators mounted on the triangular space frame. These actuators provide fine surface adjustment on a panel-by-panel

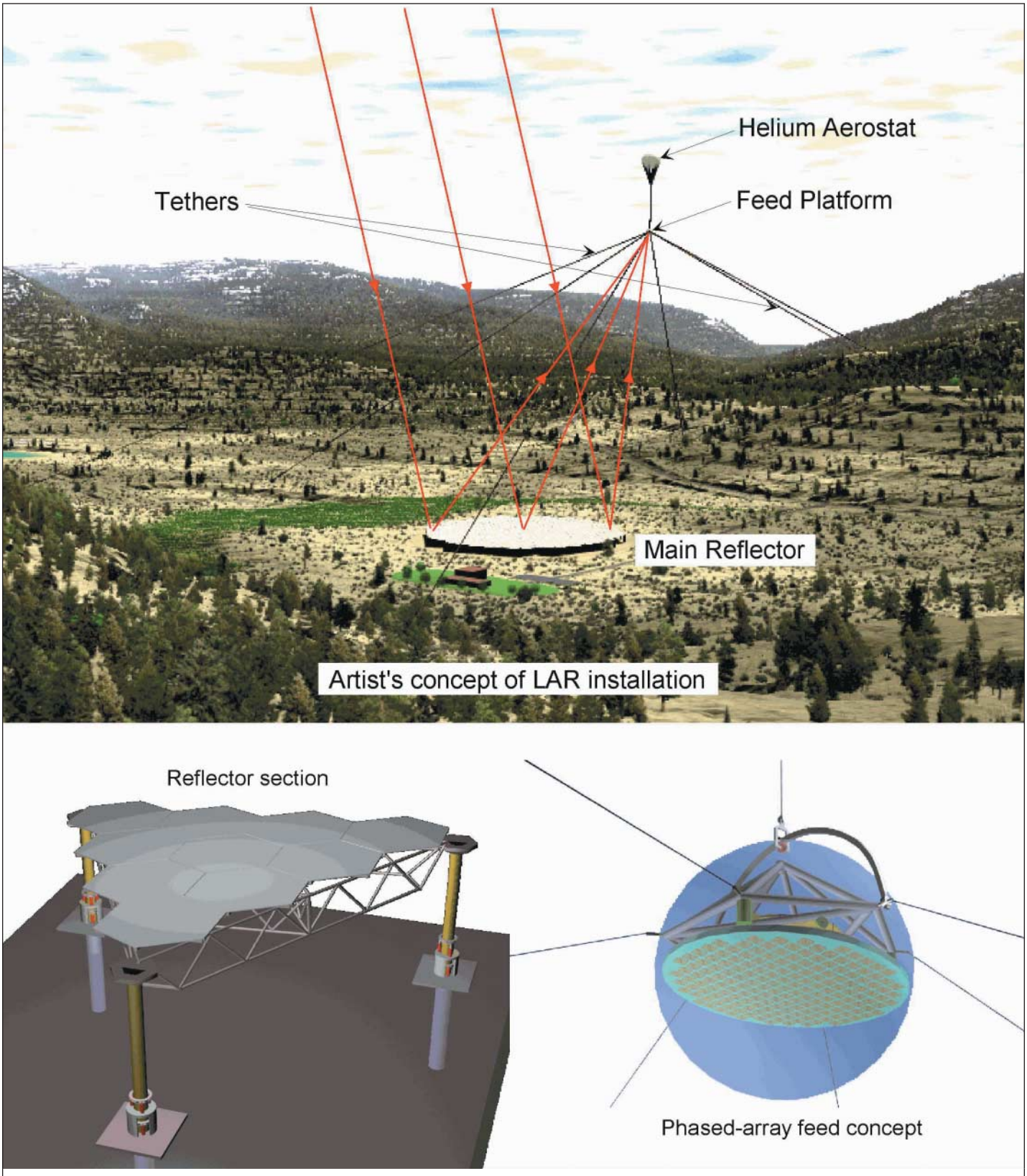

Figure 1. An artist's concept of a complete 200-m diameter LAR installation. The installation includes the main reflector, the multi-tethered aerostat system, the feed platform at focal length of 500 m. Details of a main reflector section and the prime-focus phased-array feed concept are shown at the bottom of the figure. The phased-array feed contains pointing and stabilization mechanics, phasing networks, and cryogenic coolers.

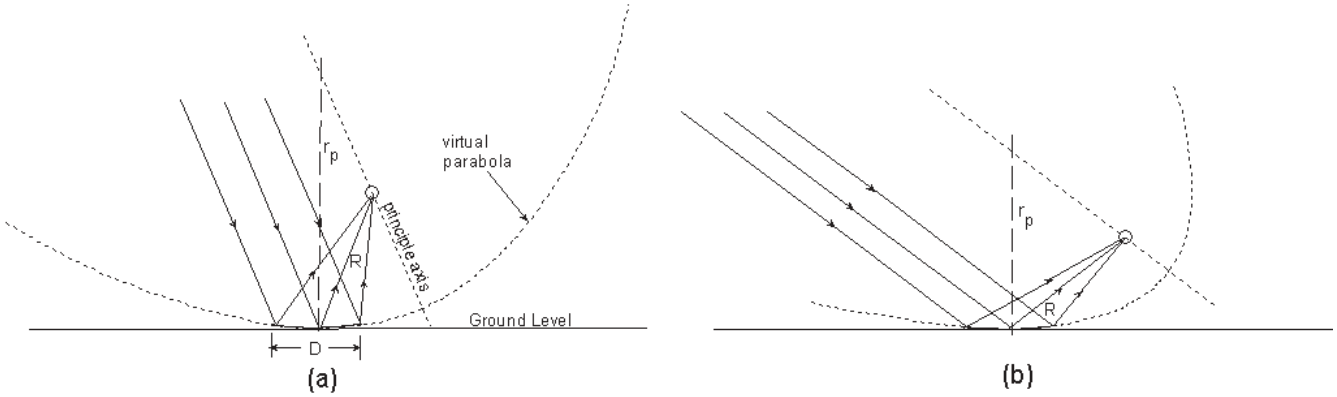

Figure 2. The LAR surface forms part of a much larger "virtual" parabola (shown in section along with its principal axis in dotted lines). For a fixed *R*, as Zenith Angle (θ_{za}) pointing changes, the height of the surface must only change a small amount along the *x*-axis (in the plane of the figure). Larger θ_{za} changes requiring larger actuator strokes occur along the *y*-axis (out of the plane of the figure) with increased zenith angle (b) since the radius of curvature (r_p in the figure) decreases.

basis, and compensate for short-term time variations that cannot be compensated for by the primary actuators. Secondary actuators will be shared by adjacent panels and positioned at the three corner-points under every panel. Currently, these actuators are expected to be ball-screw type electric actuators or fluid-filled bellows-type actuators.

2.3. Triangular Space Frame

The triangular space frame, shown in **Figures 3** and **4b**, forms the main structure onto which reflector panels are mounted. It must support the panels and maintain stability in windy conditions. Each space frame is approximately 20 m along each side, 2 m deep, with webbing constructed of 10–12 cm diameter steel pipe. The space frames are a major cost item in the reflector design and considerable effort has gone into minimizing the amount of steel used in their construction. If each triangular section of the reflector were an independent structure, then the trusses composing the sides of the triangles would run side-by-side for adjacent triangles. This redundant structure is removed in the current concept for the space frame design (**Figure 3**). Alternate triangles are replaced by bridging sections, and the amount of steel is reduced by a factor of about 1.7.

2.4. Primary (Large-Stroke) Actuator

The primary actuator design is fundamental to the construction of the main reflector. In the 200-m LAR, there will be about 100 primary actuators that are used to support and move the triangular space frames vertically. The primary actuators need to be able to support a load of several tens of tons, they must be able to support an overturning moment, they must have a stroke of up to 7 m, they must be able to slew smoothly at low speeds, and they must be inexpensive. The maximum slew rate requirement is about 2.7 mm/s for slewing the surface over its whole range in about 1 h. The maximum slew rate while tracking a radio source is less than 1 mm/s. A concept that aims to meet the above criteria is shown in **Figure 4a**.

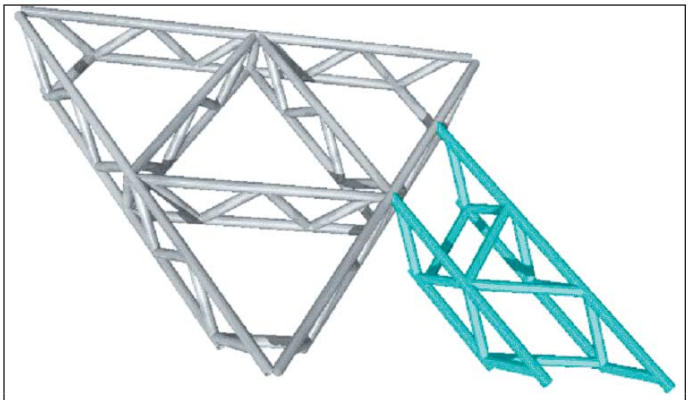

Figure 3. Triangular space frame design with bridging structure. The major triangular trusses (left of figure) form the foundation of the backup structure. They are about 20 m each side. To avoid parallel trusses running side-by-side in adjacent space-frames, alternate space-frames in the overall structure are formed by using the bridging members (right of figure). This design meets backup structure requirements with a significant reduction in steel and cost.

The actuator consists of a hollow steel pipe approximately 45 cm in diameter with 3 columns of holes in which load pins are inserted to support the pipe. The upper and lower sections contain 3 short-stroke (~30 cm) hydraulic actuators. The support column is moved by alternately engaging load pins and driving actuators in the upper and lower sections. The support column slides (with rollers not shown) into a buried guide tube in the ground. The column supports an overturning moment by ensuring that a minimum section of the support column stays in the guide tube even when fully extended.

The principal motivation for this concept is to make the cost of the actuator independent of the actuator stroke, as much as possible. A relatively small volume of the actuator is required for the motive power and complex moving parts, whereas the pipe column can be extended as long as necessary. The pipe column is moved by alternately inserting the load pins into holes at intervals in the pipe and driving upper and lower hydraulic sections. The challenge of this design is to ensure that

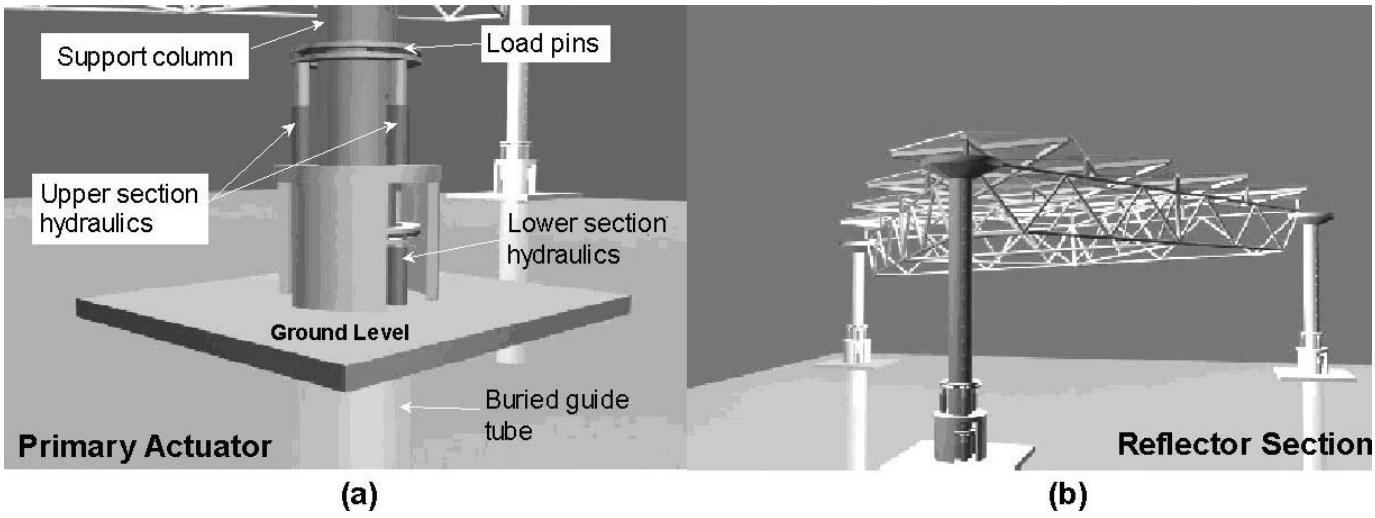

Figure 4. (a) Details of the primary actuator. (b) A triangular space frame with three supporting primary actuators.

the hand-over from one hydraulic section to another occurs as smoothly as possible (although because of the low slew rate, short interruptions in motion while hand over occurs can be absorbed by the secondary actuators).

2.5. Surface Measurement System

Because the surface comprises independently actuated panels, the position of each panel must be measured, and the results provided to the control system that is responsible for setting the surface to the commanded shape. The surface measurement system must provide rapid (~1 per second) precise (~0.5 mm) measurements of the position and orientation of the panels. There are no convenient vantage points from which to measure the surface from locations above the surface using optical or radio techniques. Constructing vantage points that would provide good triangulation angles would be expensive and difficult, and could produce aperture blockage. Additionally, above-surface multiplexed measuring schemes cannot measure the roughly 1500 panels quickly enough to track their motion while observing. Thus, the surface must be measured using devices positioned on the ground, below the reflector surface.

Two possible methods are currently being considered:

1. Short-range photogrammetry: a ground-mounted black-and-white video camera takes pictures of infrared-illuminated retro-reflective targets on the back of the panel. The position and orientation of the panel can then be deduced by analyzing the resulting image.

2. Time-of-flight laser ranging: lasers are mounted at several sites under the surface to measure the distance from the ground to retro-reflective control surfaces on the back of each panel. Each laser is directed by a mirror rotating about a vertical axis and by mirrors mounted at known positions on the ground to targets on the panels. A variation of this method has individual lasers under each panel measuring the distance directly to the panel overhead.

3. The Feed

Because the LAR uses reflective optics, its inherent frequency range is limited at short wavelengths by errors from the faceted approximation to a parabolic surface and panel surface accuracy, and at the long wavelengths by the maximum dimensions of the feed. The design goal is to cover the wavelength range from 2 m to 1.4 cm using a number of feed packages, each with approximately octave bands. The SKA also requires a field-of-view of about 1 square degree at a wavelength of 20 cm. Since an individual beam is much smaller than 1°, this requirement can only be met with a multi-beam feed.

The multi-beam, variable shape feed patterns dictate a phased-array approach to the problem at dm and cm wavelengths. At longer wavelengths, the field-of-view is large enough with only a few beams. The feeds can be thin, wire-like structures, much less dense than needed at short wavelengths. Furthermore, the required position accuracy of the feed platform is inversely proportional to the wavelength. Thus, a feed structure of order 10 m in diameter is envisioned at m wavelengths. At a 20 cm wavelength, the feed will be about 5.5 m in diameter. The mass target for the entire focal package is 1000 kg, sufficiently small to leave plenty of "excess" lift for tensioning the tethers.

3.1. Prime-Focus Phased-Array Feed

Phased-array feeds centred near a wavelength of 20 cm, the mid-frequency range of the telescope, have been studied in some detail. A phased-array feed consists of three fundamental "layers". First, there is the array, itself, composed of small (low gain) antenna elements, spaced closely together, probably in a hexagonal array on a plane. Directly behind this plane is an array of receivers. Beyond the receivers, in the signal path, is a combining network that combines the signals from the receivers to produce the required number of beams on the sky. Each beam will result from the combination of signals from a

sub-array of proximate elements. The important design decisions are to choose (i) mechanical or electronic steering for pointing of the receiver for different Zenith Angles, (ii) an element spacing, and (iii) a type of array element.

Mechanical steering has advantages. (a) Part of the mechanical-steering angle occurs "naturally" as the tensions of the tethers are adjusted for various Zenith Angles, (b) no phase shifters or delay elements are needed in the combining networks, (c) the size of the array is minimum because foreshortening at large "look angles" is avoided, (d) an element spacing of 1λ instead of 0.5λ is sufficient to avoid grating responses, and (e) there are no blind spots or other artifacts of electronic steering over large angles.

The size of the main-reflector focal region (the "spot size") is $(f/D)\lambda$. The spot must be properly sampled by the array of elements, and, in this case, the spot is larger than element spacing – thus the signals from a number of elements must be combined in a weighted sum to produce one beam on the sky. The actual number is wavelength dependent. In other words, to avoid under-illumination of the reflector at the short-wavelength end, or spillover at the long-wavelength end of the band, the number of elements summed in the combining network must be scaled with wavelength. This is a significant effect over an octave band, and indicates that the band will have to be "channelized" into sub-bands before they can be combined.

It is clear that losses in transmission lines dictate a receiver for each element. Receivers for wavelengths shorter than about 20 cm will have to be cooled to liquid-nitrogen temperatures. The size of the system, the number of interconnections, and the required signal processing strongly indicate a digital approach to the combining network. We envision the signal-processing steps to go as follows: (a) digitize the signal from each receiver, (b) digitally filter the signal into sub-bands, (c) distribute the sub-band outputs to all the summing networks that require the signal as input, and (d) form the weighted averages needed to make beams.

3.2. Mechanical Stabilization of the Feed

The feed must be stabilized to an accuracy of $\pm\lambda/4$ (for a focal ratio of 2.5) in the focal plane to maintain accurate pointing of the telescope to 1/10th of its primary beam. Orthogonal to the focal plane, the stabilization requirements are much less severe (about 5 m at 1.4 GHz), due to the large depth-of-field of the telescope. Thus, at a wavelength of 20 cm (1.4 GHz), the focal plane stabilization requirement is about 5 cm; at a wavelength of 2 m (150 MHz), it is 50 cm; at 1.4 cm (22 GHz), it is about 3.5 mm. The following factors are important in considering this problem:

1. The stability requirement scales with the size of the feed. At low frequencies where the feed is largest, and the most difficult to stabilize, the stability requirement is least stringent. At the highest frequencies where the feed is smallest, and inherently the easiest to stabilize, the stability requirement is most stringent. This relation assists the effort to adequately stabilize the feed over the entire range of observing frequencies.

2. A stabilizer need only remove the high-frequency velocity components of the feed motion—any slowly varying or constant offsets can be tracked by imparting a tilt component to the shape of the main reflector. Since the reflector is fully actuated, this does not require additional equipment.

3. An inertial stabilization system will likely be needed at the feed, since tether actuation will likely not be sufficient to obtain the required accuracies at the shortest wavelength. Such a system need not require much actuator power, since no force is needed to keep a mass from moving. A Stewart platform could be used to stabilize the feed in translation, attitude, and rotation about the principal axis of the feed. Since the tethers can be used to provide some of the orientation motion of the feed and the residual errors in position (translation) will be moderate, the ranges of motion required of the stabilization system are small. A mechanical stabilization system may not be needed at wavelengths longer than about 20 cm.

The resulting system has four levels of actuation: (1) primary actuators at the reflector, (2) secondary actuators at the reflector, (3) winch actuators, and (4) feed mechanism actuators. These are listed in terms of decreasing travel and increasing bandwidth. As such, a multi-layered control scheme will have to be designed and crossover frequencies will need to be determined at which control shifts from one level of actuation to another. As well, the design of the system must ensure that there are no gaps in the travel and (or) frequency-response characteristics of the system. Simulations of the various sub-systems are being used to determine the frequency-response characteristics, and how these are affected by various design parameters.

One of the competing SKA designs, put forward by astronomers in China, also involves a receiver suspended from cables (Su et al., 2001). However, in that case, the cables are supported by towers at the periphery of the reflector, and no aerostat is used. This design is similar to that used in the existing Arecibo telescope. Designers of that system also propose to use mechanical stabilization of the feed using a Stewart platform.

3.3. Position Measurement

The system that controls the position of the feed requires a measurement of its 3-D position, and the accuracy of this measurement will determine how well the antenna can be pointed. We propose to use differential GPS (Global Positioning System) methods, combined with a high-precision radio-based focal-distance measurement. Differential GPS is a standard technique that has been highly refined for this case. The essence of the technique is that GPS receivers are located both in known, fixed positions on the ground and on the moving feed platform, all receiving signals from the same satellites. Differential analysis of the results permits the cancellation of atmospheric propagation and selective availability effects to yield high-precision position measurements. The orientation of the feed could be measured by tilt sensors, or by using multiple

GPS receivers. Furthermore, the GPS measurements could be augmented by accelerometers and rate gyros for additional accuracy and bandwidth. The results of recent studies indicate that sub-cm measurement accuracy can be achieved. This is close to the 3.5 mm requirement for operation at a wavelength of 1.4 cm.

There are also several alternatives if GPS proves unsuitable. For example, laser-based methods could be used to accurately measure the straight-line distance to the feed platform. Three of these would provide the 3-D position. The orientation of the feed platform could then be measured using a combination of tilt sensors and rate gyros.

4. The Multi-Tethered Aerostat System

The key element of the LAR that makes it possible to build such a large offset paraboloid is its long focal length (about 500 m). This focal length and the desire to point the telescope to Zenith Angles as high as 60° at all Azimuths rules out a rigid member structure to support the feed. Instead a tension-structure is employed, similar to the guyed structures used for antenna masts. The principle of a tension-structure is that there is sufficient tension force in the tethers to offset external horizontal forces due to wind (i.e., the tethers are "pre-tensioned"). If the tethers are lightweight and there is sufficient tension, the tether profiles will be nearly straight. In this case, wind-induced forces will tend to stretch the tethers rather than changing their profile. In the case of the LAR, an aerostat provides a lifting force sufficient to maintain tension in the tethers during the worst-case operating conditions, as well as to carry the load of the feed platform.

A critical element of the success of this structure is the strength-to-weight ratio of the tether material. Strong, light cables made of such materials as Kevlar and Spectra, which have eight times the strength-to-weight ratio of steel cable, are available. Reasonably priced aerostats are also commercially available with the net lifts required (about 40 kN) for this application.

Referring to **Figure 1**, the tethered system contains several components: the tethers, the feed platform, the winches, the aerostat, and a control system (to drive the winches). The control system must maintain the feed platform, which is located at the confluence point of the tethers, at the focus of the reflector. The aerostat is offset from the confluence point by a "leash", which is about 100 m long. The leash acts as a mechanical low-pass filter that minimizes the coupling of motion of the aerostat to the feed platform. The minimum number of tethers is three. However, six tethers have been found to reduce the footprint of the telescope, to improve the Zenith Angle range at Azimuths that lie between tethers, and to increase slightly the open-loop stability of the system.

The stability of the feed/confluence point is fundamental to the feasibility of the LAR, and extensive work has been done to model its dynamical motion in gusty wind conditions. The tethers are modeled using a lumped mass approach. As well, two different types of aerostat have been modeled—streamlined and spherical, so as to evaluate their respective merits.

Since the LAR design is based on a multi-tethered aerostat, it is useful to briefly review past work on similar systems. Most prior work has dealt the more conventional configuration of an aerostat on a single tether. In that area, the work of Jones (1987), Jones and DeLaurier (1983), and Badesha and Jones (1993) stands out as the most significant and consistent contribution to the field, and we have used their work as a basis for our own simulations. In addition, two references were found dealing with an experimental study of a tri-tethered balloon (LeClaire and Rice, 1973; LeClaire and Shumacher, 1974). As expected, this system was found to have much smaller motions in response to wind disturbances than an equivalent single-tethered system.

4.1. Cable Model

In the lumped mass model, the continuous cable is first discretized into elements. The mass of each element is lumped at its endpoints (called *nodes*). The internal stiffness and damping characteristics of the cable are modeled as lumped parameter stiffness and damping elements connecting those nodes. This effectively neglects the effects of bending stiffness since the dominant forces are due to tension. This type of model, illustrated in **Figure 5**, has been validated for a variety of underwater systems with excellent agreement with in-field measurements (Driscoll et al., 2000; Lambert et al., 2003).

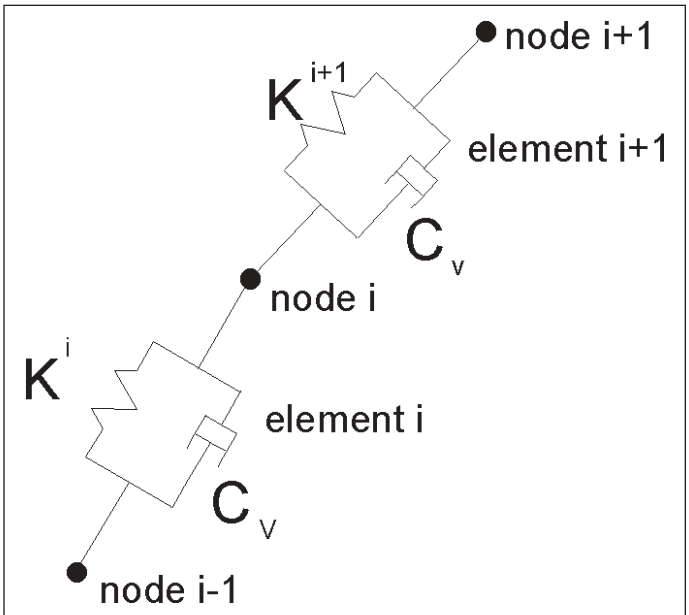

Figure 5. Cable element and node representation.

The forces in the cable model are broken down into two types: internal and external forces. Forces generated within the cable are called internal forces and are due to axial stiffness and internal damping. Forces exerted on the rope by the environment are external forces, and consist of the

aerodynamic drag and gravitational forces. The tension in the cable due to its axial stiffness is considered to act only in the tangential direction and is modeled by a linear function relating tension and strain. The tension is set to zero if the strain becomes negative. However, this condition was never reached in the cases investigated since the aerostat buoyancy is very large in relation to the weight of the system aloft. The friction between the braids of the cable tends to create a damping effect. The resulting force is assumed to be linear with strain rate.

The external forces acting on the cable element are those due to aerodynamic drag and gravity. The drag forces acting on the cable element can be calculated based on the element's drag coefficient and the velocity of the element's geometric centre relative to the surrounding air. These velocities must account not only for the motion of the cable element, but also the motion of the surrounding air (to be discussed in a later section). The drag coefficient is modified by appropriate loading functions (Driscoll and Nahon, 1996), which are functions of the relative angle between the *i*th element and the incident fluid flow. These loading functions account for the nonlinear breakup of drag between the normal and tangential directions. Once the drag for elements i and $i + 1$ are calculated, half of each value is applied to the ith node which joins the two elements. Finally, the net gravitational force acting on a cable element is calculated based on the element's volume and density.

The equations for internal forces and the drag forces are developed in an elemental body-fixed frame, while the equations for the gravitational forces are developed in an inertial frame. The motion equations are written in the inertial frame, and thus all forces are transformed into that frame prior to inclusion in these equations.

4.2. Aerostat Model

The aerostat design for LAR has not yet been finalized—it may be spherical or streamlined. Models for both these types of aerostat are therefore considered here. Based on a prior statics analysis of the LAR system (Fitzsimmons et al., 2000), it was expected that the spherical aerostat would not perform as well due to its higher drag coefficient. However, the spherical aerostat would be cheaper to purchase and operate, and so was considered worth investigating.

4.2.1. Spherical Aerostat

The spherical aerostat is modeled as a single mass at the upper node of the leash, subject to buoyancy, aerodynamic drag (generated by winds and gusts), and gravity. Its aerodynamic drag can be found based on its drag coefficient and the local velocity of its geometric centre relative to the surrounding air. The variation in drag coefficient of a spherical object (McCormick, 1995), from 0.4 to 0.15 depending on the Reynolds number of the flow, was incorporated into the simulation.

The added mass of the aerostat was included in the model since it is significant. This was calculated as half the displaced air mass of the corresponding spheres (Newman, 1989). The antenna receiver, located at the upper confluence point of the three tethers, is assumed to be enclosed in a spherical housing, and its aerodynamic drag is therefore found using a similar approach.

4.2.2. Streamlined Aerostat

The streamlined aerostat modeled is a scaled-up (by a factor of 2.33) version of the Aeros FlightCam aerostat, shown in **Figure 6**. The aerostat in **Figure 6** is being used in a proof-of-concept demonstration for this project, and will be discussed in more detail in the next section. For modelling purposes, the aerostat is considered to be rigid and capable of 6 degrees of freedom motion. The model uses a component breakdown method, as outlined by Nahon (1996). The aerostat is considered to be composed of the hull and three aft fins. The forces acting on the aerostat are due to aerodynamics, weight, and buoyancy. Both weight and buoyancy act along the vertical and their values are considered constant. The aerodynamic forces are calculated for each single component, and later summed.

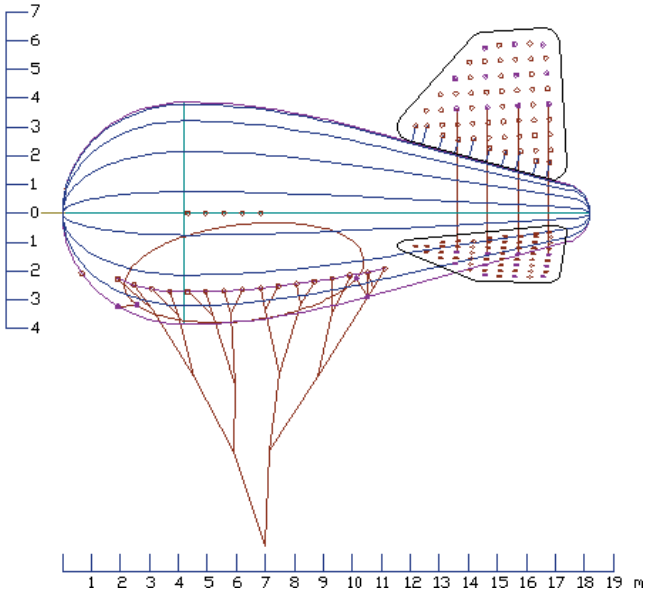

Figure 6. Aeros FlightCam aerostat.

The location of the centre of pressure of the fins is approximated at their 1/4 chord line midway from the base to the tip. The fins are approximated as NACA 0018 sections and the dimensionless lift coefficient is calculated using available empirical data for airfoil shapes. The lift coefficient is then reduced to account for (a) the finite aspect ratio of the fin, and (b) the reduction in fin effectiveness due to operation in the disturbed airflow at the rear of the hull. The drag coefficient of the fins is computed as the sum of its parasite and induced-drag coefficients (McCormick, 1995). The lift and drag forces are then calculated using the lift and drag coefficients.

The method of Jones and DeLaurier (1983) is used to calculate the hull's lift and drag forces as well as the pitch

moment about the nose. The effective point of application of the hull force is then calculated from the hull moment and lift force. Once all forces are found, they are summed to obtain the total force acting on the aerostat. The moments exerted by these forces are also summed to obtain the total moment acting on the aerostat.

4.3. Wind Model

A wind model was incorporated to determine its effect on the tethered aerostat system. It consists of a height-dependent mean-wind profile on which are superimposed turbulent gusts that also vary with height. The mean wind U at height h was represented by a power law profile (Etkin, 1972) representing the Earth's boundary layer where the power-law exponent $\alpha = 0.19$ was used to represent conditions in rural areas. A gradient height $h_g = 500$ m was used, at which the mean wind reaches its full speed of U_g.

Turbulent gusts were superimposed on this mean wind using a von Kàrmàn model (Etkin, 1972) for atmospheric turbulence in the planetary boundary layer. Other properties, such as turbulence intensities were selected to represent typical neutrally stable atmospheric conditions in a rural setting (Etkin, 1972). The turbulence intensities in the three orthogonal directions were varied with altitude, as were the three corresponding scale lengths.

4.4. Controller

Winches at the base of each tether are used to keep the receiver in the desired position in the presence of wind and turbulence. Each winch is controlled by an independent PID controller that responds to errors in the receiver position, which we presume to be accurately measured. A planar representation of the geometry is shown in **Figure 7**.

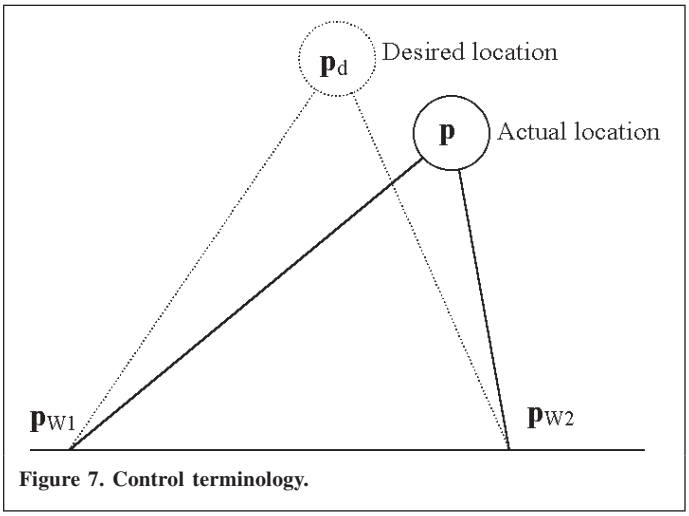

Figure 7. Control terminology.

The desired location of the receiver is at $\mathbf{p}_d$ while its actual location is at $\mathbf{p}$. The location of the jth winch ($j = 1,\ldots,3$) is at $\mathbf{p}_{Wj}$. For each winch, we can, therefore, define the error in the receiver position as

$$e_j = \|\mathbf{p} - \mathbf{p}_{Wj}\| - \|\mathbf{p}_d - \mathbf{p}_{Wj}\|$$

Our winch controller can now operate according to

$$\Delta L_j = -(k_P e_j + k_D \dot{e}_j + k_I \int e_j \, dt) \quad j = 1,\ldots,3$$

where ΔL_j is the change in length of tether j, and k_P, k_D, and k_I are, respectively, the proportional, derivative, and integral gains. The three gains are the same for all tethers, as no advantage was found for them to be different.

The motivation behind this approach is that, if the distance from winch j to the receiver is correct, then the receiver lies on a sphere of radius L_d^j centred at the winch. If all three receiver-winch distances are correct, then the receiver lies at the intersection of those spheres that define the correct desired location of the receiver in 3-D space. To limit the winch power requirements, a bound of 50 kW was imposed that had to be satisfied throughout the operating envelope and cases considered.

4.5. Simulation Results

Results are presented here for a case with three tethers, the streamlined aerostat, and a 100 m leash. The receiver's desired position was at a fixed point on a hemisphere of radius $R = 500$ m whose centre lay on the Earth's surface. The winches were each located 1200 m from the hemisphere's centre and configured symmetrically 120° apart. **Figure 8** shows a comparison of errors and tensions for $\theta_{za} = \theta_{az} = 0$, $U_g = 10$ m/s, $\theta_w = 0$, gains = 5, 3, 1, with and without control. The motion is plotted as components in and out of the focal plane (the plane locally tangent to the 500 m hemisphere at the desired aerostat location). When $\theta_{za} = \theta_{az} = 0$, the focal plane is horizontal and the out-of-plane motion is purely vertical. For this configuration with control, the maximum error is 36.5 cm, while its maximum component in the focal plane is an order of magnitude less. The uncontrolled case makes it apparent that the system responds little to high-frequency gusts and acts as a natural low-pass filter due to its huge scale.

In general, we have found that the positioning error can be consistently kept below 85 cm throughout the operating envelope. Of course, with more power available at the winches, the control gains could be increased and the ensuing positioning errors would be further reduced.

The same gains were applied to the system operating with the spherical aerostat. The maximum error and the power required were found to be much lower than for the streamlined aerostat. The error could be further reduced by increasing the gains until the 50 kW power limit is reached.

A statics analysis of the LAR system (Fitzsimmons et al., 2000) indicates that the streamlined aerostat should lead to *better* system performance. Consistent with that investigation, we found that the steady-state forces are generally lower for the streamlined aerostat. However, the *variations* about the mean, which are a more important issue for dynamic positioning, were higher, due to the aerodynamic lift generated by the hull

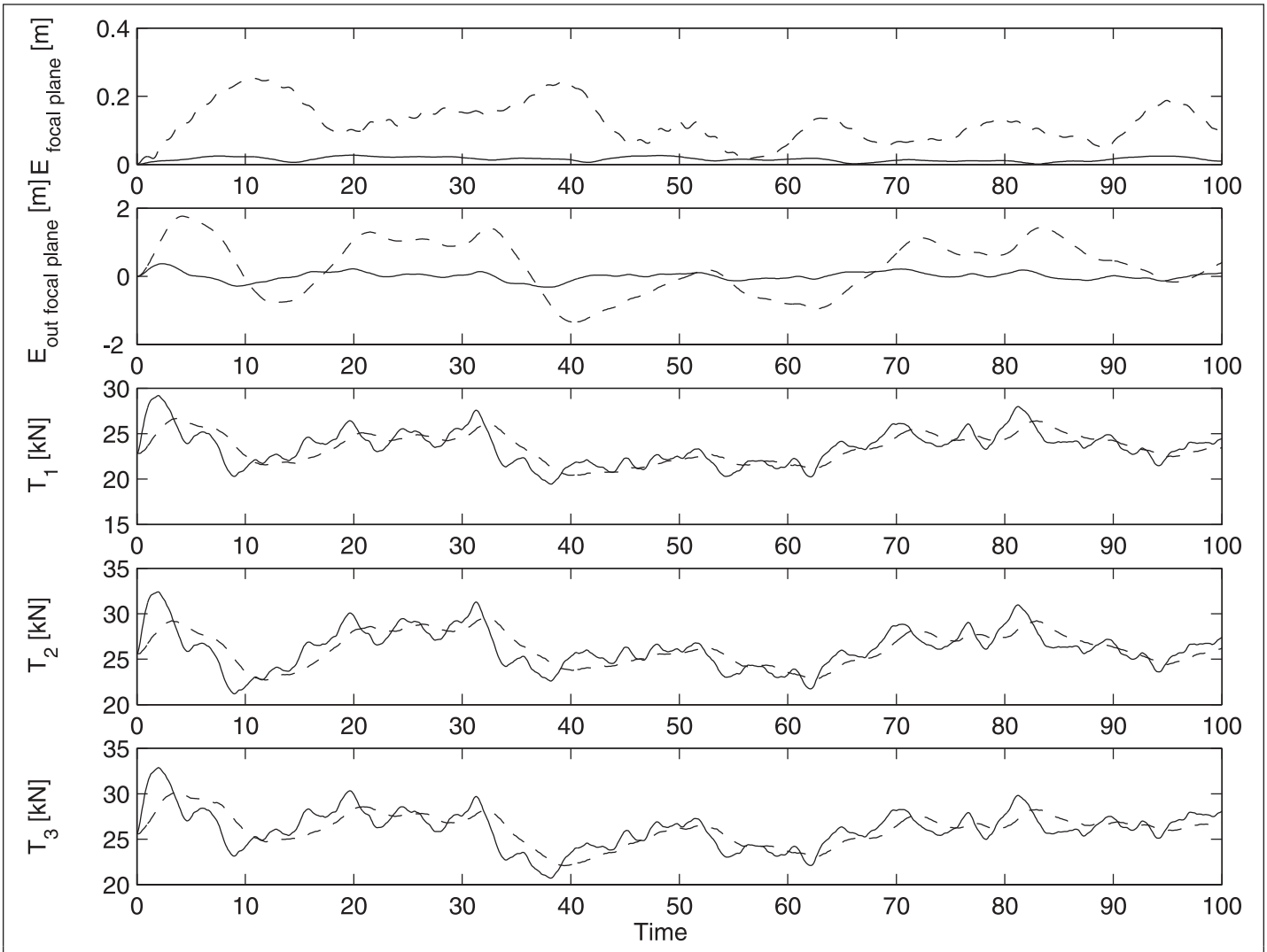

Figure 8. Comparison of errors and tensions with control (continuous line) and without control (broken line). For these plots, $\theta_{za} = \theta_{az} = 0$, $U_g = 10$ m/s, $\theta_w = 0$, and gains = 5, 3, 1.

and fins. It should be noted though, that this simulation does not include the effects of vortex shedding from the spherical aerostat – a phenomenon that would cause additional disturbances (Govardhan and Williamson, 1997; Lambert, 2002).

5. Proof-of-Concept Prototype

The tethered aerostat subsystem is arguably the highest risk component of the LAR design. To complement the intensive modeling and simulation investigation focussed on that subsystem, a scaled prototype is being constructed in Penticton, B.C. This prototype will also allow us to gain operational experience with a large aerostat. A scale factor of 1/3 was chosen as a good compromise between cost and closeness to full size. Systematic scaling (Lambert, 2002) was used to determine the desired properties of the scaled system, so that the experimental results obtained with it would be analogous to the full-scale system. Some variation on those parameters was required to satisfy criteria such as off-the-shelf availability of components, and safety issues.

A streamlined aerostat was purchased from Aeros FlightCam, and it is shown during initial flight trials in **Figure 9**.

Facilities have been constructed in Penticton to allow the deployment and testing of the multi-tethered subsystem. These include a trailer (**Figure 9**) with winch to transport the aerostat between points on the site, a hangar (**Figure 10**) to house the aerostat when it is not being used, and a shed that houses the control computer and electrical junctions.

The test facility will not include a reflector or receiver, since its main purpose is to validate the multi-tethered aerostat concept. In place of the receiver, an instrument housing (shown in **Figure 11**) will be attached at the confluence point of the tethers. This housing contains a GPS receiver and accompanying radio modem, a load cell on each tether, tilt sensors, a magnetic compass, a temperature sensor, wind-speed and wind-direction sensors, A/D converters for all instruments,

Figure 9. Early flight trial of the Aeros streamlined aerostat.

Figure 10. Hangar in Penticton, B.C.

an RS485-RS232 converter, a radio modem for data other than GPS, and power supplies. This suite of instruments will allow us to collect sufficient data to understand the system's behaviour, and to validate the results of our computer simulation. Once the simulation is validated, it can be used with greater confidence when simulating the full-scale system.

The deployment of the aerostat is scheduled in the following phases:

1. Initial deployment of the aerostat on a single tether using one manually-controlled winch. To gain experience with the behaviour of the aerostat in various wind conditions and to determine best procedures for launching and recovering the aerostat. This phase was completed in April 2002.

2. Deployment of the aerostat on a tri-tether arrangement, with fixed-length perimeter tethers, and without instruments. To gain experience with the aerostat in a tri-tether arrangement, and to determine best procedures for launching and recovering the aerostat. This phase was completed in May 2002.

3. Deployment on a tri-tether arrangement, with fixed-length perimeter tethers, with the instrument package. To gather data on the open-loop behaviour of the tri-tether system in various configurations (different tether lengths). This phase was completed in October 2002.

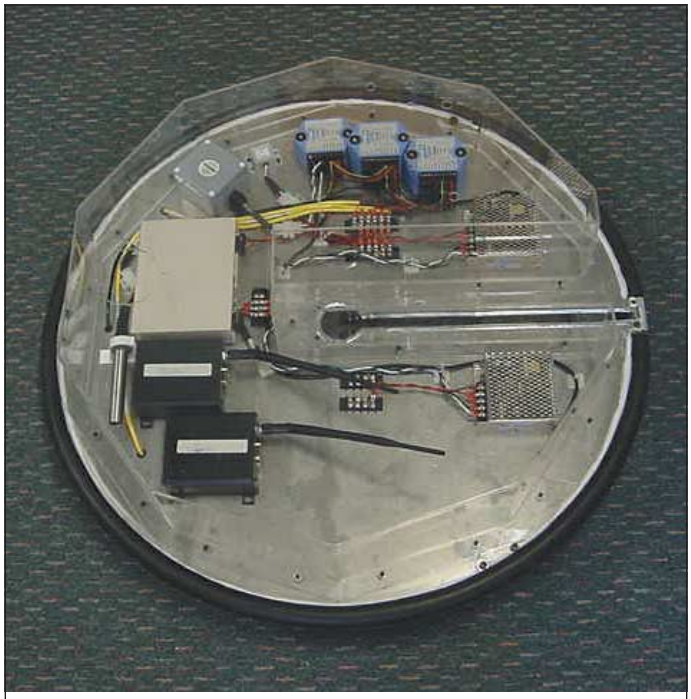

Figure 11. Instrument housing.

4. Development and deployment of the computer-controlled winches and control system for the outer tethers. This phase is ongoing in late 2002, and will continue into early 2003.

5. Deployment on a tri-tether arrangement with winches on the outer tethers, under manual control. To determine the behaviour of the system as tethers are varied in length. This phase will be conducted in February 2003.

6. Deployment on a tri-tether arrangement with winches on outer tethers, under computer control. To determine the behaviour of the system and to gather data under closed-loop control. This phase should be conducted in March—May 2003.

7. Deployment on a 6-tether arrangement, first open-loop, and then with winches under computer control. To determine the behaviour of this system, and to gather data. This phase is expected in the second half of 2003.

The results obtained to date have been very satisfactory in terms of stability of the system motion. The aerostat appears very stable, especially when it is at altitude, on a long leash (150 m). When on a short leash, it becomes more difficult to handle, especially near the ground in high winds. In fact, gaining experience with these operational issues is one of the main purposes of this proof-of-concept experiment.

In total, the test program is expected to last about 2 years. By the end of this period, we will have gained a good understanding of the system's behaviour, in practice; we will have validated our computer simulation, and we hope to answer the crucial question: *will it work* ?

6. Conclusions

The Large Adaptive Reflector represents Canada's design for the Square Kilometer Array. One complete installation includes a 200 m reflector, a receiver, and a multi-tethered aerostat subsystem to support the receiver. Initial paper studies have been completed showing that all components are feasible, and that the performance of the system is promising. Using winches at the base of the tethers, we expect to position the receiver within a 1 m envelope, even in strong winds. The remaining precise positioning will be performed by an inertially-stabilized mechanism mounted at the confluence point. The next stage involves construction of some of the key components, such as the multi-tethered aerostat subsystem, to prove the concept in practice.

Acknowledgments

Funding for this research was provided by a grant from the National Research Council of Canada and the Canada Foundation for Innovation.

References

Badesha, S., and Jones, S.P. (1993). "Aerodynamics of the TCOM 71M Aerostat". AIAA Paper No. 93-4036-CP.

Carlson, B., Dewdney, P., Veidt, B., Fitzsimmons, J., Nahon, M., Stiemer, S.F., Chang, K., Halliday, D., Lo, D., Lachapelle, G., Cannon, E., Shafai, L., Mousavi, P., and Belostoski, L. (2000). "Large Adaptive Reflector: A 200-m Diameter Wideband cm-wave Radio Telescope". *Proceedings of the SPIE International Symposium on Astronomical Telescopes and Instrumentation 2000*, Munich, Germany. March 2000. pp. 33–44.

Driscoll, F., and Nahon, M. (1996). "Mathematical Modeling and Simulation of a Moored Buoy System". *Proceedings of OCEANS'96 MTS/IEEE*, 1996. pp. 517–523.

Driscoll, F., Lueck, R., and Nahon, M. (2000). "Development and Validation of a Lumped-Mass Dynamics Model of a Deep-Sea ROV System". *Appl. Ocean Res*. Vol. 22, No. 3, pp. 169–182.

Etkin, B. (1972). "Dynamics of Atmospheric Flight", John Wiley & Sons, New York.

Fitzsimmons, J.,Veidt, B., and Dewdney, P. (2000). "Steady-State Analysis of the Multi-tethered Aerostat Platform for the Large Adaptive Reflector Telescope". *Proceedings of the SPIE International Symposium on Astronomical Telescopes and Instrumentation 2000*, Munich, Germany. March 2000. pp. 476–488.

Gordon, W.E., and Lalonde, L.M. (1961). "The Design and Capabilities of an Ionospheric Radar Probe". *IRE Trans. Antennas Propag*. Vol. AP-9, pp. 17–22.

Govardhan, R., and Williamson, C.H.K. (1997). "Vortex-Induced Motions of a Tethered Sphere". *J. Wind Eng. Industrial Aerodynam*. Vol. 69–71, pp. 375–385.

Jones, S.P. (1987). "Nonlinear Dynamic Simulation of a Moored Aerostat". AIAA Paper No. 87-2505.

Jones, S.P., and DeLaurier, J.D. (1983). "Aerodynamic Estimation Techniques for Aerostats and Airships". *AIAA J. Aircraft*, Vol. 20, No. 2, pp. 120–126.

Lambert, C. (2002). "Dynamics Modeling and Conceptual Design of a Multi-tethered Aerostat System". M.Sc. thesis, Department of Mechanical Engineering, University of Victoria, Victoria, British Columbia.

Lambert, C., Nahon, M., Buckham, B., and Seto, M. (2003). "Dynamics and Control of Towed Underwater Vehicle System, Part II: Model Validation and Turn Maneuver Optimization". *Ocean Eng*. Vol. 30, No. 4, pp. 47–48.

LeClaire, R.C., and Rice, C.B. (1973). "The Local Motions of a Payload Supported by a Tri-tethered Natural Shape Balloon". US Air Force Report AFCRL-TR-73-0748.

LeClaire, R.C., and Shumacher, H.L. (1974). "Local Motions of a Payload Supported by a NOLARO Tri-Tethered Balloon". *Proceedings of the Eighth AFCRL Scientific Balloon Symposium*, October 1974. pp. 233–255.

Legg, T.H. (1998). "A Proposed New Design for a Large Radio Telescope". *Astron. Astrophys*. Supplement Series 130, pp. 369–379.

B.W. McCormick. (1995). "Aerodynamics, Aeronautics and Flight Mechanics", John Wiley & Sons, 1995.

Nahon, M. (1996). "A Simplified Dynamics Model for Autonomous Underwater Vehicles". *Proceedings of the 1996 IEEE Symposium on Autonomous Underwater Vehicle Technology,* 1996. pp. 373–379.

Newman, J.N. (1989). "Marine Hydrodynamics", MIT Press,.

Su, Y.X., Duan, B.Y., Nan, R.D., and Peng, B. (2001). "Development of a Large Parallel-Cable Manipulator for the Feed-Supporting System of a Next-Generation Large Radio Telescope". *J. Robotic Syst*. Vol. 18, No. 11, pp. 633–643.

